Bull Volcanol (2006) 68: 653–670
DOI 10.1007/s00445-005-0040-7

RESEARCH ARTICLE

Marco Laiolo · Corrado Cigolini

Mafic and ultramafic xenoliths in San Bartolo lava field: New insights on the ascent and storage of Stromboli magmas

Received: 10 December 2002 / Accepted: 29 August 2005 / Published online: 13 January 2006

Abstract Mafic and ultramafic xenoliths are well represented within a large basaltic lava field of Stromboli. These basalts, known as San Bartolo lavas, show a high-K calc-alkaline (HKCA) affinity and were erupted <5 ka BP. Xenoliths consist of olivin-gabbro, gabbronorite, anorthosite, dunite, wehrlite and clinopyroxenite. Thermobarometric estimates for the crystallization of gabbroic materials show minima equilibration pressures of 0.17–0.24 GPa, at temperatures ranging from 940 to 1,030°C. These materials interacted with hydrous ascending HKCA basaltic magmas (with temperatures of 1,050–1,100°C) at pressures of about 0.2–0.4 GPa. These pressure regimes are nearly identical to those found for the crystallization of phenocrystic phases within HKCA basaltic lavas. Gabbroic inclusions are regarded as cumulates and represent crystallized portions of earlier HKCA Strombolian basalts.

Dunite and wehrlite show porphyroclastic-heterogranular textures, whereas the clinopyroxenite exhibit a mosaic-equigranular texture typical of mantle peridotites. These ultramafic materials are in equilibrium with more primitive basaltic magmas (under moderately hydrous and anhydrous conditions) at pressures of 0.8–1.2 GPa, which is below the crust-mantle transition, located at about 20 km depth under Stromboli.

Major and trace element distributions indicate *comagmatism* between the host basaltic lava and the mafic and ultramafic inclusions. REE patterns for mafic nodules are relatively regular and overlap the field of basaltic lavas (HKCA). They show moderate to high LREE enrichments and moderate enrichments in HREE relative to chonrites. Spider diagrams also show significant similarities between the lavas and the mafic-ultramafic xenoliths as well.

During their ascent, primitive Strombolian magmas may be stored in upper-mantle regions where they interact with peridotitic materials and partly differentiate (to give dunite and wehrlite) before migrating to upper crustal levels. In this region, hydrous basaltic magmas (with estimated water contents of 2–3.5 wt%) are stored in the subvolcanic environment, and are allowed to crystallize the gabbroic materials before reaching the surface under nearly anhydrous conditions.

Keywords Basaltic magma · Xenoliths · Rock-melt interactions · Thermobarometry

Editorial responsibility: R. Cioni

M. Laiolo (✉) · C. Cigolini
Dipartimento di Scienze Mineralogiche e Petrologiche,
Università di Torino,
V. Valperga Caluso 35,
10125 Torino, Italy
e-mail: marco.laiolo@unito.it

Introduction

The Aeolian arc (Southern Italy) is very peculiar since a close petrogenetic link is likely to exist between high-K calc-alkaline and shoshonitic lavas, and both lava types have erupted from the same volcano (such as at Stromboli) or from contiguous volcanic centers (i.e., at Vulcano) (Barberi et al. 1974; Francalanci et al. 1993a; De Astis et al. 1997). Stromboli is the north-eastern island of the Aeolian arc; the cone of the volcano rises 924 m a.s.l. and was formed during the last 100,000 years (Gillot and Keller 1993). Recent activity has been strombolian, with continuous explosions and eruptions of scoriae, lapilli, ash and bombs (e.g., Francalanci et al. 1999; Rosi et al. 2000). Typical explosions are essentially associated with a continuous escape of gases from the open conduit (Allard et al. 1994). Barberi et al. (1993) pointed out that the persistent Strombolian activity may be interrupted by lava effusions, major explosions and paroxysms (the latter events being often coeval with the generation of tsunamis). During the last century several lava flows were erupted onto the "Sciara del Fuoco" (up to a total of 18 episodes, cf. Nappi 1976; for the description and chronology of the first 17). Before the last effusive activity (started on December 28, 2002 and continued until July 21, 2003), that was accompanied by

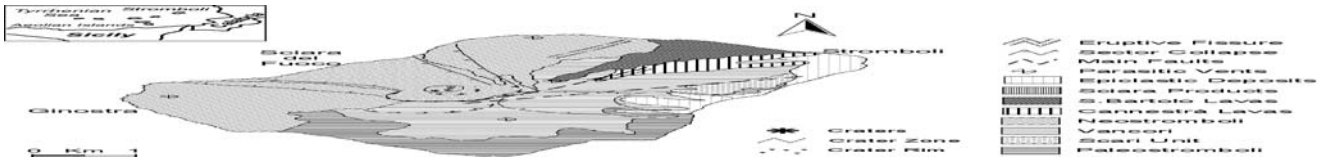

Fig. 1 Simplified geologic map of Stromboli (modified from Keller et al. 1993 and Finizola et al. 2002). Note the San Bartolo lava field in the NE sector of the island

a major explosion (on April 5, 2003), previous lava flows were erupted in 1985–86 and 1975, respectively (cf. Nappi 1976; De Fino et al. 1988).

The volcanic cone of Stromboli has been subdivided into five major units (Hornig-Kjarsgaard et al. 1993). These are reported in Fig. 1 together with other minor units mapped by Keller et al. (1993). The first three major units make the older part of the volcano, known as *Paleostromboli* . The fourth is named *Neostromboli* and is located along the northern and western sectors of the island, whereas the so-called *Recent Stromboli* refers to the recent lavas and tephra erupted onto the northeastern side (San Bartolo lavas) and the Sciara del Fuoco (a NW collapsed sector delimited by two upward convergent scarps). K/Ar dating by Gillot and Keller (1993) show that even the lower units of Paleostromboli are relatively young. Older lavas and tephra (Paleostromboli I, 110–85 ka in age) are basalts, basaltic andesites and andesites belonging to high-K calc-alkaline (HKCA) series and are overlain by the volcanic rocks, of similar type, of Paleostromboli II (64–55 ka) with transitional characteristics from alkaline (CA) to high calc-alkaline (HKCA). The lavas and tephra of Paleostromboli III (35±6 ka) are on top of this sequence, and consists of basaltic andesites, andesites of the high K calc-alkaline (HKCA) series, and shoshonites. The youngest rocks of Paleostromboli are overlain by the partly altered lavas and tephra of the Scari unit (of basaltic and shoshonitic composition). The Vancori sequence (ranging from basalts to trachytes with shoshonitic affinity and age from 26 to 13 ka) lays on top of these rocks that, in turn, are overlain by the lavas and tephra of Neostromboli (13–6 ka). These may bear leucite in their groundmass and belong to the so-called potassic series (KS), as summarised by Francalanci et al. (1989, 1993a).

Present day activity is taking place along the "Sciara del Fuoco", and consists of high-K calc-alkaline to shoshonitic lavas and tephra. Recent San Bartolo lavas, erupted from a parasitic vent NE of the present crater, are basaltic in composition and are thought to be younger than 5 ka. These lavas were erupted as a composite lava field (extended for about 0.65 km^2) onto the Vancori lavas and the Canestrà lava field (shoshonitic basalts of the Neostromboli unit) exposed the northern sector of the island. Stratigraphic relationships between the San Bartolo lavas and the other materials of Recent Stromboli are unknown.

Cognate monzonitic and accidental xenoliths found within the Neostromboli tephra (belonging to the KS series) were described by Renzulli and Santi (1997). Moreover, Renzulli et al. (2001, 2003), Vaggelli et al. (2003) and Mattioli et al. (2003) reported several types of cognate (gabbroes) and accidental xenoliths (tonalite, diorite, quartzite and high-grade hornfelses) within the lavas of Paleostromboli I and II, respectively.

In this paper we will provide new petrochemical data and textural observations on earlier Stromboli basaltic lavas and associated mafic and ultramafic nodules. The occurrence of these materials allows us to decode interaction processes which occur during magma ascent and storage and, by means of thermobarometry, to constrain the depth of the magma chamber. This reservoir plays a crucial role in modulating magma ascent through the "open conduit" of Stromboli, whose internal dynamics is strictly linked to the activation of major explosive eruptions (cf. Barberi et al. 1993; Bonaccorso et al. 1996; Bertagnini et al. 1999; Coltelli et al. 1999; Ripepe and Gordeev 1999; Métrich et al. 2001; Bertagnini et al. 2003). The understanding of the "root zone" of the feeding system may also throw light on the petrogenesis of the associated magmas.

Analythical methods

Mineral phases were analysed at the University of Turin (Department of Mineralogy and Petrology) with a fully automated Cambridge SEM-EDS microanalyzer using natural and synthetic standards. Mineral analyses were performed using a finely focused beam. Glasses were analysed under a relatively broad beam (15 μm in diameter). Data have been corrected for background, drift, mass absorption and secondary fluorescence according to the ZAF method. The relative errors are within 5% for most of major elements and may go up to 10% for minor elements (with concentrations <1.00 wt%).

Bulk chemical analyses on selected rock-samples were obtained on selected lavas by means of a ICP-AES spectrometer at the "Centre de Recherches Pétrographiques et Géochimiques du CNRS" (at Vandoeuvres, Nancy, France). Trace and REE data were determined by a ICP-MS spectrometer at this institution. Analytical precision is 2-3% for concentrations up to 100 ppm, 3–6% in the range 10–100 ppm, and 6–10% at and below 10 ppm, respectively.

Petrography and mineral compositions

In this section we will outline the petrography and the mineral compositions of San Bartolo lavas and associated mafic and ultramafic xenoliths. These volcanics are exposed in the north-eastern sector of Stromboli and were erupted

Table 1 Summary of the petrographic characteristics of mafic and ultramafic xenoliths found in San Bartolo lavas compared with other xenolithic suites at Stromboli

Suite	Host lava (relative age)	Type	Texture	Assemblage	Peculiarities	Ref.
Mafic xenoliths	S. Bartolo lavas (<5 ka)	gabbro	orthocumulitic heterogranular	Pl, Cpx±Ol, Mt, glass	presence of interstitial glass	1
	S. Bartolo lavas (<5 ka)	gabbronorite	orthocumulitic heterogranular	Pl, Cpx, Opx Ol, Mt, glass	coronas of cpx±opx±mt on ol	1
	S. Bartolo lavas (<5 ka)	gabbro-anorthosite	orthocumulitic heterogranular	Pl±Cpx±Hbl±Phl, Mt, glass	deformation twinning & mylonitic textures	1
	Petrazza tephra, Paleostromboli I (110–85 ka)	gabbro	cumulate textures	Pl, Cpx, ol±Hbl±Mt±Bt	holocrystalline groundmass	2
Ultramafic xenoliths	S. Bartolo lavas (<5 ka)	dunite	porphyroclastic & protogranular	Ol, Cr-spinel	strain lamellae in olivine	1
	S. Bartolo lavas (<5 ka)	wherlite	porphyroclastic & protogranular	Ol, Cpx, Cr-spinel	deformation bands & twinning in ol	1
	S. Bartolo lavas (<5 ka)	clinopyroxenite	mosaic equigranular	Cpx±Cr-spinel	dihedral grain boundaries	1
Other xenoliths	Ash deposits above Neostromboli (13–0.5 ka)	monzonite	orthocumulate-poikilitic	Sa, Pl, Cpx, Ol, Phl, Mt	poikilitic large sanidine crystals (up to 4 mm in size)	3
	Omo lava flow Paleostromboli II (64–55 ka)	diorite-tonalite	hypidiomorphic heterogranular	Pl±Kfs±Qtz±Bt, Mt, glass	interstitial glass	4
	Petrazza tephra, Paleostromboli I (110–85 ka)	granophyre	micrographic and myrmekitic	San, Pl, Qtz±Opx±Cpx±Phl±Mt	coarse micrographic intergrowths	4
	Petrazza tephra, Paleostromboli I (110–85 ka)	rhyolitic obsidian	quenched assemblage on a glassy matrix	Sa+Bt	quenched microlites on colorless glass	4
	Omo lava flow Paleostromboli II (64–55 ka)	quarzite	granoblastic-poligonal textures	Qtz, Kfs, Cpx, Bt±Ms±Ep±Zrn	re-crystallized restitic quartz	5
	Omo lava flow Paleostromboli II (64–55 ka)	high-grade hornfelses	fine to medium holocrystalline rocks	anorthoclase, Crd, Hc, Sil±Crn	hornfelses related to a contact aureole	6

References: 1, this work; 2, Mattioli et al. (2003); 3, Renzulli and Santi (1997); 4, Renzulli et al. (2000); 5, Vaggelli et al. (2003); 6, Renzulli et al. (2003)
Abbreviations for mineral phases are from Kretz (1983)

Table 2 modal percentage[a] of minerals within selected mafic and ultramafic xenoliths

Sample	Str4	Str22	Str15	Str21	Str19
Type	gabbro	gabbro	gabbroanorthosite	wherlite	wherlite
plagioclase	51.4	38	77.1	–	–
clinopyroxene	34.3	48.2	6.1	46.9	48.6
olivine	10	7.7	16.8	52.5	50.7
spinel	1.2	tr	tr	0.6	0.7
apatite	tr	tr	tr	–	–
glass	3.1	6.1	tr	–	–

Abbreviations: tr: traces

[a]1,000 points counted

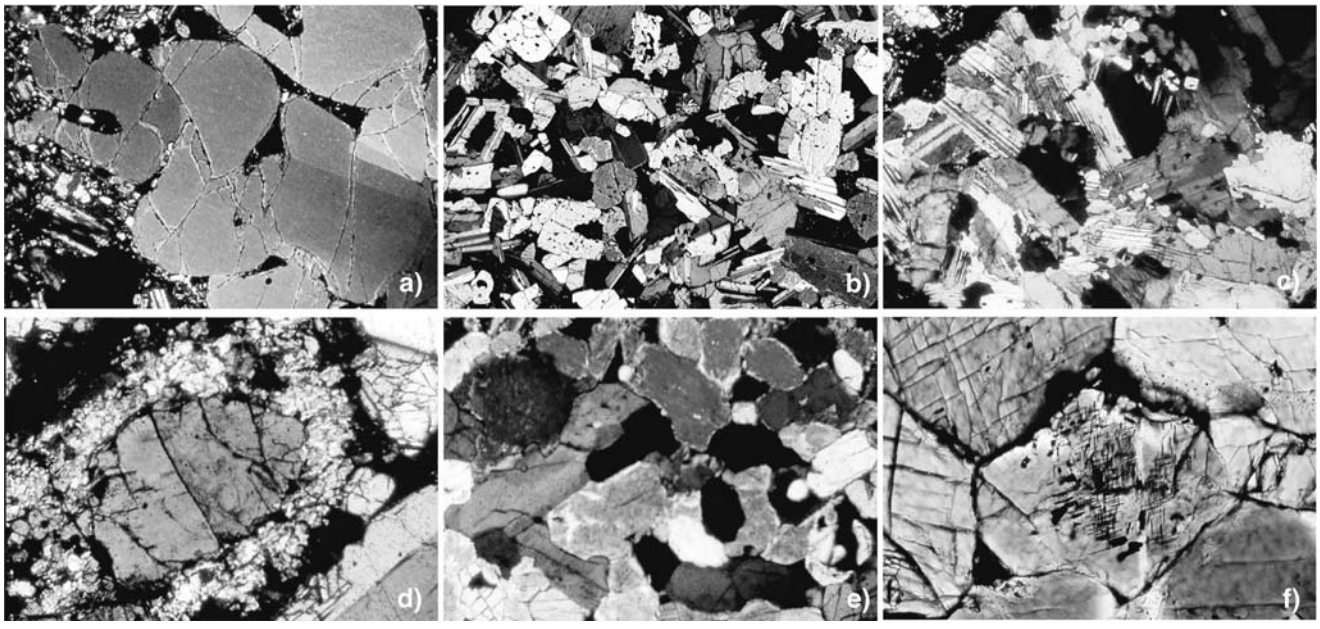

Fig. 2 Microphotographs summarizing the petrographic and textural features of Strombolian lavas and associated xenoliths. **a)** Xenocryst of forsteritic olivine in San Bartolo lavas with clear deformation bands. The xenocryst shows evidence of resorption due to reaction of the forsteritic olivine with the host melt. Crossed polarizers. Long dimension: 4.2 mm. **b)** Orthocumulate heterogranular texture in an anorthositic xenolith. Weakly mylonitic textures visible in several plagioclase laths and are the result of brittle deformations within the crust. Crossed polarizers. Long dimension: 4.2 mm. **c)** Deformation twinning in plagioclase in contact with clinopyroxene within a gabbroic xenolith. Crossed polarizers. Long dimension: 1.2 mm. **d)** Corona of granular clinopyoxene and subordinate orthopyroxene rimming olivine within a gabbronoritic xenolith. Crossed polarizers. Long dimension: 1.2 mm. **e)** Mosaic equigranular texture within a clinopyroxenitic xenolith. Note the dihedral angles among contiguous recrystallized crystals. Crossed polarizers. Long dimension: 4.2 mm. **f)** Needles of ilmenite in clinopyroxene of a wehrlitic xenoliths. Note the triple junctions among recrystallized grains. Crossed polarizers. Long dimension: 1.2 mm

as a massive lava field onto the rocks of Neostromboli. Petrographycally they are essentially HKCA porphyritic basalts. In Table 1 we provide the synopsis of the different types of xenoliths found at Stromboli. Modal abundances for selected mafic and ultramafic xenoliths are given in Table 2.

Host lavas

Sampled lavas exhibit a seriate porphyritic to glomeroporphyric texture, with a high porphyrity index (up to 40–45%). Plagioclase is the most abundant phase with subordinate clinopyroxene, olivine and orthopyroxene. Accessory phases consist of abundant titano-magnetite, and apatite. Groundmass textures are typically pilotaxitic to microfelsitic-granular textures. Crystal clots of gabbroic, gabbronoritic and "anorthositic" type are abundant within San Bartolo lava field and are dispersed within the lavas together with xenocrysts of olivine (Fig. 2a) and anorthitic plagioclase.

Plagioclase phenocrysts, of anorthitic to labradoritic composition (An_{90-75}, Table 3, Fig. 3), are euhedral to subhedral and show normal zoning with typical *sieve textures*. Only few crystal show reverse zoning from bytownite to anorthite at their rim. *Clinopyroxene* of augitic composition (En_{57-52} and $Wo_{40\pm2}$) is the most abundant mafic phase (Table 4, Fig. 4) and may form, in association with olivine, cumulophyric crystal clots. Some crystals are more diopsidic (En_{48-46} and $Wo_{48\pm2}$). Al_2O_3 contents vary from 2–3.5 wt% (with the Ca-Tschermak molecule ranging from 2 to 6%) and TiO_2 values are always $\leq$1 wt%.

Olivine crystals are microphenocrysts and microlites, generally subhedral, normally ranging from Fo_{75} to Fo_{68} (Table 5, Fig. 5). Megacrysts and xenocrystic aggre-

Table 3 Selected SEM-EDS analyses of plagioclase

	Lavas								Mafic xenoliths					
Sample	St2	St2	Stl8	Stl8	St21	St21	St21	Stl5	St4	St4	Stl8	Stl8	Stl5	Stl5
site	core	nm	core	nm	core	int	nm	gdm	core	nm	core	nm	core	nm
SiO_2	49.2	49.0	46.5	47.1	45.9	47.6	49.9	52.6	44.9	44.1	44.5	44.8	45.8	51.2
Al_2O_3	32.6	32.7	34.1	34.1	34.4	33.0	31.6	29.5	34.5	34.4	36.6	35.9	34.1	31.4
FeO[a]	0.97	0.92	1.02	0.52	0.41	0.59	0.82	1.38	1.03	0.68	0.40	0.09	0.37	0.42
CaO	14.6	14.7	17.1	17.1	17.9	16.4	15.0	11.9	18.7	19.1	19.0	18.6	17.1	13.7
Na_2O	2.82	2.45	1.72	1.94	1.22	2.08	2.80	4.73	0.91	0.72	0.81	0.97	1.84	3.64
K_2O	0.31	0.32	n.d.	0.04	n.d.	0.18	0.28	0.51	n.d.	0.12	0.09	0.03	0.13	0.30
Total	100.50	100.05	100.48	100.77	99.78	99.86	100.34	100.56	99.91	99.06	101.33	100.46	99.32	100.66
Ab	0.25	0.23	0.15	0.17	0.11	0.19	0.25	0.41	0.08	0.06	0.07	0.09	0.16	0.32
An	0.73	0.75	0.85	0.83	0.89	0.81	0.74	0.56	0.92	0.93	0.92	0.91	0.83	0.66
Or	0.02	0.02	–	–	–	0.01	0.02	0.03	–	0.01	0.01	–	0.01	0.02

[a]total iron as FeO

Abbreviations: gdm: groundmass; n.d.: not detected

gates of olivine, with a highly forsteritic composition (Fo_{84}-Fo_{90}) have been occasionally found (Fig. 2a). They show *deformation bands and twinning* typical of mantle peridotites (Mercier and Nicolas 1975; Conticelli and Peccerillo 1990). *Orthopyroxene* is found as anhedral to subhedral microphenocrysts occasionally associated with olivine phenocrysts. Locally it may rim clinopyroxene phenocrysts. It is essentially hypersthene with En_{68-55} and $Wo_{3\pm0.4}$ (Table 4). The olivine-orthopyroxene Fe-Mg distribution coefficient ($K_D = X^{opx}_{Mg} X^{ol}_{Fe} / X^{opx}_{Fe} X^{ol}_{Mg}$) is rather constant and ranges 0.81–0.85 for the olivine compositions within the higher frequency mode reported in Fig. 5 (Fo_{70-75}). This parameter when calculated for clinopyroxene-olivine is more variable (0.9–1.3), but it stabilizes around 1.2–1.3 for an olivine composition of Fo_{80-82}. Therefore olivines of this composition seem to crystallise during the earlier stages of evolution of S.Bartolo magma and/or were partly inherited from disaggregation of mafic and ultramafic materials.

Well-developed subhedral and anhedral crystals of *titaniferous magnetite* have 5–12 wt% TiO_2 with average compositions of $Mt_{80\pm10}Usp_{20\pm10}$ (Table 6).

Mafic xenoliths

We selected 15 samples of mafic xenoliths which exhibit a round to angular shape, they are essentially gabbro, gabbronorite and gabbroanorthosite exhibiting a preserved orthocumulitic heterogranular texture (Fig. 2b). Their sizes range from 2 to 6 cm across, and most of the samples have variable amounts of interstitial brownish glass.

Plagioclase crystals are euhedral to subhedral and may show normal-oscillatory zoning. Their compositions range from anorthite to labradorite (An_{90-66}, Table 3, Fig. 3). Some gabbroic and anorthositic samples show *deformation twinning* and weakly *mylonitic textures* (Fig. 2c) similar to those found in the mafic xenoliths of Arenal volcano (Costa Rica) (Cigolini and Kudo 1987). *Clinopyroxene* crystals are euhedral to subhedral with a diopsidic composition straddling the augite field (see Table 4, Fig. 4). Al_2O_3 contents vary from 1.4 to 5 wt% (with the Ca-Tschermak molecule ranging from about 1.5 to 7%). In gabbronoritic samples, this phase is coexisting with *olivine* and *titano-magnetite* to form *coronitic textures* (Fig. 2d). These textures have been interpreted as a product of subsolidus reactions (between plagioclase and olivine) typical of metagabbros of the granulite facies (cf. Gardner and Robins 1974; Cigolini and Kudo 1987).

Olivine is generally subhedral and, in few cases, anhedral with a rather variable composition from sample to sample (Fo_{74}–Fo_{82}) (see Table 5, Fig. 5). CaO and MnO contents are lower than those found in volcanic rocks (<0.35 wt%).

Orthopyroxene is well represented in gabbronorites, being essentially bronzite-hypersthene (En_{72-80} and $Wo_{2.8\pm0.5}$). It exhibits an euhedral to subhedral shape and it may be found in coronitic textures rimming olivine crystals, as well (Fig. 2d).

Amphibole (of pargasitic composition) and *phlogopite* (with $Mg/Fe^{++} \sim 0.85$) are present as inclusions in clinopyroxene crystals of a gabbroanorthositic sample (Table 7). Accessory phases are essentially *titaniferous-magnetite*

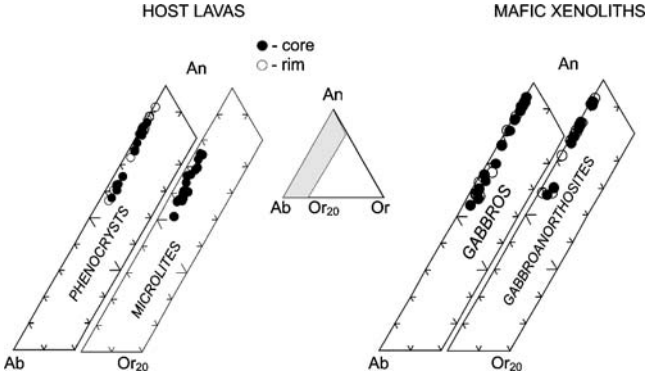

Fig. 3 Ternary diagram showing plagioclase compositions for recent Strombolian lavas and gabbroic xenoliths. Symbols: *black dots* are cores, *open circles* are rims

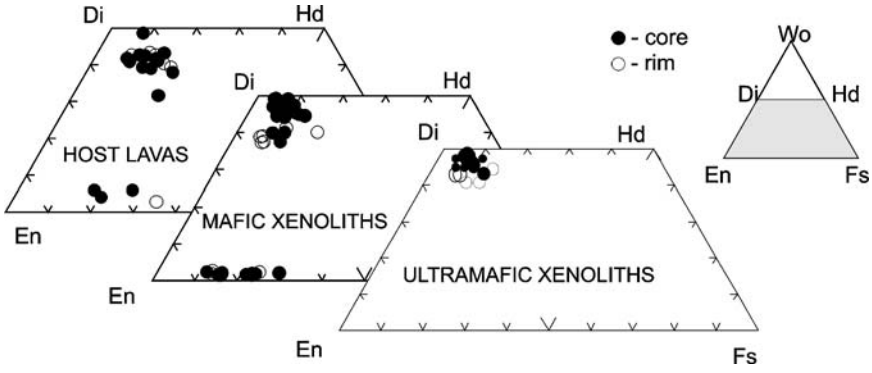

Fig. 4 Pyroxene quadrilateral showing the compositions of clinopyroxenes and orthopyroxenes found within the recent lavas, mafic and ultramafic xenoliths. Symbols: *black dots*, cores; *open circles*, rims

($Mt_{75\pm10}Usp_{25\pm10}$) and *apatite*, normally included in plagioclase and clinopyroxene (Table 6).

Ultramafic xenoliths

We selected 12 ultramafic xenoliths which are represented by dunites, wehrlites and clinopyroxenites. They have round to prysmatic shapes ranging from 1 to 4 cm. Dunites and wehrlites show porphyroclastic inequigranular textures with local relict domains of protogranular type (i.e., Mercier and Nicolas 1975). Only in one case we found a clinopyroxenite with a mosaic equigranular texture (Fig. 2e). Interstitial glasses are absent.

Olivine in dunites and wehrlites are large (up to 2–5 mm across) and may display clear deformation bands and twinnings. As previously mentioned, this feature is typical of mantle peridotites. Within the dunites, olivine shows a forsteritic composition (Fo_{90}–Fo_{88}), whereas in wehrlite has a wider compositional range Fo_{89}–Fo_{80} (i.e., Table 5, Fig. 5). Clinopyroxene in wehrlites, similar in size with coexisting olivine crystals, is euhedral to subhedral and shows a diopsidic compositions with higher Cr_2O_3 and Al_2O_3 contents (the latter up to 6 wt%, cf. Table 4), whereas in pyroxenes of clinopyroxenite Al_2O_3 is low (1.2–2.6 wt%).

Cr-rich spinels (with $Cr_2O_3 \approx 40$–50% and Cr#, defined as Cr/[Cr+Al], ranging from 0.57 to 0.65) are normally found as microinclusions in olivine and clinopyroxene (Table 6, Fig. 6). Needles of sagenitic ilmenite have been rarely found in some clinopyroxene (Fig. 2f). An additional accessory phase is acicular apatite essentially in olivine.

Glass compositions

We have analysed the glasses in the mesostasis of San Bartolo basaltic lavas, as well as that found in interstitial domains within the gabbroic inclusions (Table 8). Most of the lava glasses plot within the andesite and trachyandesite field of the TAS diagram (Le Maitre et al. 1989; Fig. 7) with several straddling the trachydacite field. Their Mg# numbers (defined as $Mg/Mg+Fe^{+2}$) are relatively low ($\leq$0.35). However, Métrich et al. (2001) found more primitive melt inclusions (of basaltic and trachybasaltic compositions) within olivines of recently erupted scoriae with Mg# between 0.55 and 0.50. Interstitial glass of gabbroic inclusions is rather variable in silica and total alkalies with Mg#$\leq$0.43. Some of these straddle the rhyolitic field with a silica content up to 72.6 wt% and Mg# values down to 30.

When plotted onto the K_2O vs. SiO_2 diagram of Peccerillo and Taylor (1976) few lava glasses plot within the HKCA field showing an andesitic composition (Fig. 7b). However, the great majority of both interstitial glasses (lavas and gabbroic xenoliths) exhibit a marked K_2O enrichment typical of the postassic series. This is particularly evident for the trachytic melts. As we will later discuss, this further support comagmatism between these xenoliths and San Bartolo lavas.

Major and trace element compositions

Major and trace elements data have been obtained on San Bartolo lavas and are reported in Tables 9 and 10, together with some additional samples collected from flows inside the "Sciara del Fuoco" in 1985 and 1975. Additional data include the analyses of the selected *gabbroic* and *ultramafic xenoliths* hosted in San Bartolo lava flow.

Major elements

San Bartolo lavas are by far the less evolved lavas sampled on the island. In particular the silica content ranges from about 49.3 up to 51.1 wt% with moderate variations in terms of total iron. When compared to 1975 and 1985 lavas, TiO_2 and P_2O_5 are slightly lower in San Bartolo basalts. MgO is relatively constant ($\sim$7 wt%) whereas CaO is higher in other recent lavas (erupted in 1975–1985; cf. Table 9). When plotted on the K_2O vs. SiO_2 diagram of Peccerillo and Taylor (1976), San Bartolo lavas fall in the HKCA suite whereas, as already shown by Francalanci et al. (1989; 1993a) and Hornig-Kijarsgaard et al. (1993), the 1975 and 1985 lava flows have a distinct shoshonitic affinity (e.g., Nappi 1976; Capaldi et al. 1978; De Fino et al. 1988) similar to present-day scoriae and pumices (Métrich et al. 2001; Bertagnini et al. 2003; Francalanci et al. 2004).

Table 4 Selected SEM-EDS analyses of clinopyroxene and orthopyroxene

	Lavas							Gabbroic xenoliths					Ultramafic xenoliths			
Sample	St2	St2	St21	St21	St21	St21	St2	St4	St4	St18	St18	St18	St21	St21	St36	St36
site	core	rim	core	int	rim	gdm	in (pl)	core	rim	core	rim	corona	corona	core	rim	core	rim
SiO_2	51.3	51.6	52.3	51.9	52.0	51.7	53.5	50.4	49.1	52.5	51.3	54.5	55.3	52.1	52.2	55.1	51.8
TiO_2	0.63	0.47	0.53	0.69	0.38	0.43	0.34	0.33	0.62	0.41	0.41	0.37	n.d.	0.09	0.17	n.d.	0.31
Cr_2O_3	n.d.	0.06	n.d.	0.20	0.36	0.23	n.d.	0.18	0.43	0.33	0.43	0.18	n.d.	0.24	0.32	0.81	0.28
Al_2O_3	2.92	3.47	2.17	2.88	3.42	3.17	1.31	4.17	4.93	3.25	3.60	2.07	1.83	2.34	3.31	1.40	2.54
Fe_2O_3	0.97	1.66	1.30	1.30	0.55	1.12	n.d.	2.18	3.67	0.79	2.01	n.d.	1.14	1.24	0.55	n.d.	1.14
FeO	8.58	4.99	8.05	8.12	3.68	7.27	16.1	4.15	4.67	5.07	4.86	5.88	12.4	4.46	5.01	3.13	6.48
MnO	0.37	0.08	0.37	0.17	0.10	0.06	0.88	0.23	0.20	0.35	0.15	0.31	0.58	n.d.	0.13	0.09	0.14
MgO	14.5	15.4	15.6	14.6	16.1	15.3	25.3	14.7	14.0	15.0	14.9	18.1	28.4	15.8	15.4	18.0	15.7
CaO	19.4	21.3	19.9	20.4	22.8	19.9	1.29	22.3	21.6	22.4	22.3	19.0	1.10	22.1	22.0	22.2	20.7
Na_2O	0.51	0.65	0.38	0.52	0.26	0.57	0.48	0.54	0.68	0.52	0.48	0.38	0.38	0.41	0.42	0.04	0.35
Total	99.20	99.67	100.64	100.79	99.60	99.81	99.21	99.17	99.90	100.56	100.45	100.69	101.10	98.76	99.44	100.78	99.45
Wo	0.36	0.38	0.37	0.37	0.41	0.36	0.35	0.39	0.36	0.41	0.39	0.36	0.02	0.41	0.40	0.42	0.38
En	0.41	0.43	0.43	0.40	0.44	0.42	0.47	0.41	0.40	0.41	0.41	0.49	0.73	0.44	0.42	0.48	0.44
Fs	0.13	0.08	0.13	0.13	0.06	0.11	0.13	0.07	0.07	0.08	0.08	0.09	0.18	0.07	0.08	0.05	0.10

Fe_2O_3 calculated according to the stoichiometry

Abbreviations: *gdm*: groundmass; *in*: included in plagioclase (*pl*); n.d.: not detected

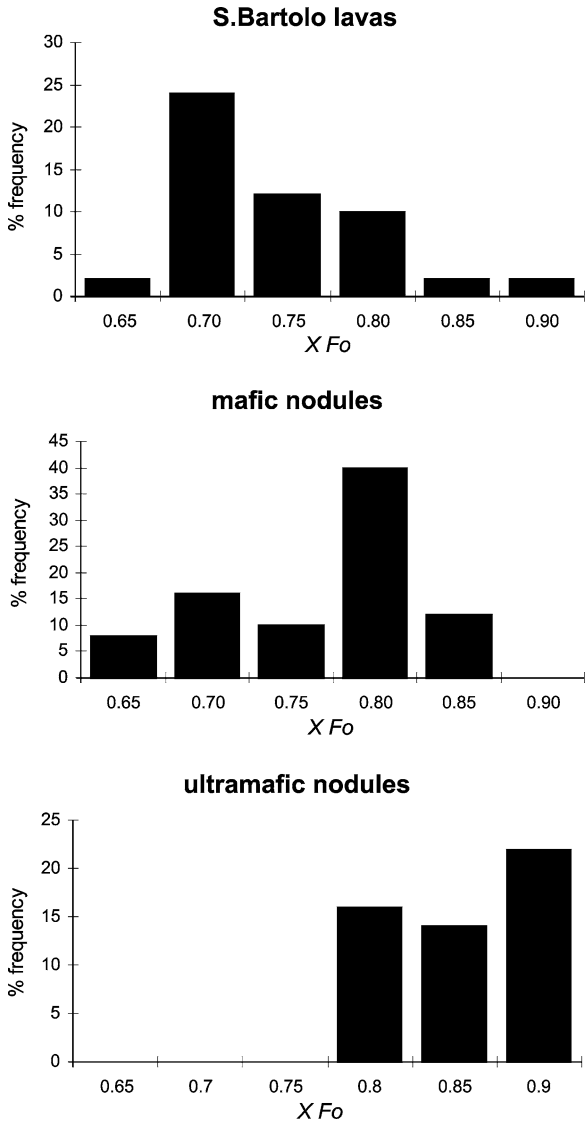

Fig. 5 Histograms showing olivine compositions within San Bartolo basalts and the associated mafic and ultramafic xenoliths. See text for details

Analyzed *olivine gabbroes and gabbroanorthosite* are hypersthene normative. These xenoliths have a variable content in Al_2O_3, up to 21.7 wt% in the gabbroanorthosite. Alkalies within the gabbroic xenoliths are slightly higher than those found in the low-K basaltic andesites of Arenal (Costa Rica), whereas their contents in anorthosite are rather similar (cf. Beard and Borgia 1989; Cigolini 1998).

The MgO content in *dunite* reaches 47.8 wt%, and is higher than silica (~40%). In this sample the occurrence of alumina (0.52 wt%) may be ascribed to the presence of microinclusions of Cr-spinel (cf. Table 6).

Compared to dunite the analyzed *wehrlite* has a slightly higher SiO_2 content, and higher contents in Al_2O_3, CaO and FeO due to the presence of abundant clinopyroxene as well as Cr-spinel. MgO contents are obviously lower (28.6 wt%).

The *clinopyroxenite*, consisting essentially of recrystallized diopsidic pyroxene, resembles the major element mineral chemistry of this mineral phase (cf. Table 4).

Trace elements

The analyzed lavas show Rb/Sr ratios ranging from 0.086–0.090 (1975 and 1985 lavas) to 0.118 (San Bartolo basalts). In particular, 1975–1985 lavas show Rb/Sr ratios similar to those of the pumices erupted on August 23, 1998 (Métrich et al. 2001). REE patterns for the effusive materials (Fig. 8a) are relatively "regular" with enrichments in LREE up to two orders of magnitude above reference chondrites, whereas HREE show only moderate enrichments (around 10 to 20 times). Shoshonitic lavas erupted in 1975 and 1985, with ($[La/Lu]_N$ ranging from 12.96 to 15.34), are slightly more enriched when compared to the HKCA San Bartolo lavas (with $[La/Lu]_N$=10.30–11.30). We may notice that *gabbroic xenoliths* have similar patterns (Fig. 8b) with variable degrees of enrichments (with $[La/Lu]_N$ ranging from 16 to 9). One of the analyzed gabbros is slightly more enriched, whereas the *gabbroanorthosite* shows lower contents in all REE due to the lack of interstitial glass. The lavas show small negative anomalies in Ce and very little negative anomalies in Eu and Er.

These characteristics are also present in the patterns outlined by the mafic xenoliths, with the exception of the gabbroanorthosite, which shows a clear positive Eu anomaly, due to plagioclase abundance. The *ultramafic xenoliths* have similar patterns (Fig. 8a), although less enriched in most of trace elements, and are therefore interpreted as "comagmatic" with the above lavas and gabbroic inclusions. The degree of enrichments in several trace elements in wehrlite and dunite is likely due to the presence of needles of apatite in both rocks and rutile-ilmenite in wehrlite (Fig. 8a and 9a). Moreover, it is not excluded that the higher enrichment in LREE within the clinopyroxenite is associated with recrystallization and re-equilibration at depth (cf. its mosaic-equigranular texture), coupled with the extraction of a melt phase (which would directly lower the LREE distribution coefficients, e.g., Wood and Blundy 1997; 2002), before being included in San Bartolo basalt.

Spider diagrams (normalized to primordial mantle values, according to Wood et al. 1979) for the lavas and the ultramafic nodules are also very similar (Fig. 9a). Common features, also recorded by the gabbroic nodules

Table 5 Selected SEM-EDS representative analysis of olivine

	Lavas					Gabbroic xenoliths				Ultramafic xenoliths			
Sample	St5	St5	St15	St15	St15	St15	St15	St18	St18	St7	St17	St21	St21
site	core	core	core	rim	gdm	core	rim	core	rim	core	core	core	rim
SiO_2	40.2	39.8	38.3	38.4	41.5	40.6	38.4	39.1	39.7	41.3	41.1	40.0	39.7
FeO[a]	19.7	21.6	24.6	25.3	10.8	15.8	22.4	21.9	18.3	12.5	9.60	18.8	19.5
MnO	0.44	0.31	0.35	0.37	0.33	0.35	0.23	0.27	0.29	n.d.	0.24	0.61	0.39
MgO	39.7	38.4	35.0	34.8	46.9	42.5	37.0	38.2	41.1	46.5	47.7	40.6	40.7
CaO	0.20	0.35	0.25	0.34	0.24	0.16	0.30	n.d.	0.22	0.25	0.32	0.14	n.d.
Total	100.31	100.44	98.41	99.12	99.65	99.45	98.36	99.40	99.56	100.52	98.96	100.04	100.23
Fo	0.77	0.75	0.71	0.70	0.87	0.81	0.74	0.75	0.79	0.86	0.89	0.79	0.79

[a]total iron as FeO; *gdm*: groundmass; n.d.: not detected

Table 6 Selected SEM-EDS analysis of spinels

	Lavas			Gabbroic xenoliths					Ultramafic xenoliths				
Sample	St2	St15	St15	St4	St5	St18	St18	Sample	St7	St7	St19	St21	St21
site	gdm	in (ol)	in (pl)	in (pl)	in (ol)	core	core	site	core	rim	core	core	in (ol)
TiO_2	12.64	7.65	4.40	10.3	11.9	3.9	5.85	TiO_2	n.d.	n.d.	4.43	8.51	0.63
Cr_2O_3	0.17	nd	0.15	0.63	0.25	0.11	0.17	Cr_2O_3	53.0	46.8	28.8	24.4	42.7
Al_2O_3	2.63	3.19	2.17	3.85	3.02	4.04	4.66	$A1_2O_3$	14.0	18.3	8.47	8.64	18.6
Fe_2O_3	38.77	49.7	56.4	44.7	42.9	53.0	48.4	Fe_2O_3	5.56	7.66	21.3	20.1	8.86
FeO	38.50	32.0	27.7	35.3	37.1	31.3	32.04	FeO	16.0	14.8	25.3	28.3	16.6
MnO	0.45	0.42	0.52	0.47	0.87	0.36	0.16	MnO	n.d.	n.d.	0.42	0.18	n.d.
MgO	1.27	3.15	3.33	4.36	2.97	1.64	2.83	MgO	11.4	12.5	6.82	7.79	11.9
CaO	0.37	n.d.	n.d.	0.28	0.07	0.06	0.39	CaO	0.13	n.d.	0.23	0.14	0.46
Total	94.80	96.09	94.63	99.87	99.02	94.39	94.49	Total	100.11	100.12	95.68	98.08	99.71
Mt	0.57	0.71	0.83	0.61	0.56	0.86	0.78	Cr number	0.72	0.63	0.70	0.65	0.61
Usp	0.43	0.29	0.17	0.39	0.44	0.14	0.22						

Fe_2O_3 calculated according to their stoichiometry

Abbreviation: *gdm*: groundmass; *in*: inclusions in olivine (*ol*) and plagioclase (*pl*); n.d.: not detected

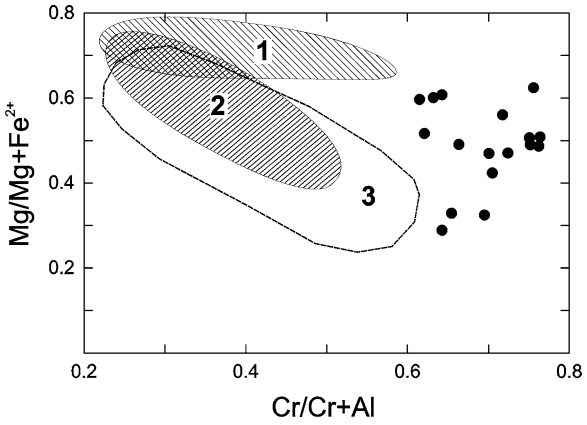

Fig. 6 Distribution of Cr-spinels found in the ultramafic materials plotted on the Mg/Mg+Fe^{2+} versus Cr/Cr+Al (Cr#). (1) Lherzolite and harzburgite xenoliths within Monte Vulsini lavas (Conticelli and Peccerillo 1990), (2) western Alps lherzolite from the Voltri Massif (Ernst 1978; Ernst and Piccardo 1979), (3) xenoliths in ophiolites at convergent plate boundaries (Cabanes and Mercier 1988)

(Fig. 9b), are the marked negative anomalies at Rb, Hf and Ti which is typical of orogenic suites in island arcs. Slight positive anomalies are observed for Th, La, Sm and Tb. Other peculiarities include a positive anomaly at Sr for the gabbroanorthosite that, in turn, is reversed to a negative anomaly in the ultramafic xenoliths and a pyroxene rich gabbro. A typical characteristic of Stromboli lavas, and related "xenoliths", is the relatively high contents of HFSE when compared to lavas found in other Aeolian islands (as pointed out by Francalanci et al. 1989; 1993a; Ellam et al. 1989; De Astis et al. 1997; Peccerillo 1999; 2001).

On petrogenetic grounds, trace element distributions are intermediate between arc magmas and intraplate compositions, resembling OIB-like signatures (e.g., Calanchi et al. 2002; Peccerillo 1999, 2001). These features has been largely debated in recent literature, and have been related to the presence of plume material within arc environments (Marquez et al. 1999) or, alternatively, they might be simply due to low degrees of partial melting of the mantle wedge partly contaminated by slab components (Reiners et al. 2000).

Geothermometry and oxygen fugacities

Geothermometric estimates on lavas and xenoliths have been obtained by applying several geothermometers, which take into account specific equilibrium assemblages.

We utilized the two-pyroxene geothermometer by running the computer code QUILF (Andersen et al. 1993) to estimate equilibrium temperatures for the crystallization of the lavas and the gabbroic inclusions. It can be noticed that San Bartolo lavas yield temperatures of about 1,050–1,130°C that are considerably higher than those estimated for the gabbroic inclusions (that do not exceed 1,030°C, see Table 11). Moreover, there is a basic consistency between the results obtained by applying the cited methods.

Table 7 Selected SEM-EDS analysis of phlogopite and amphibole from gabbroanorthosite

Phlogopite			Amphibole		
Sample site	St13 in (cpx)	St13 in (cpx)	Sample site	St13 in (cpx)	St13 in (cpx)
SiO_2	39.7	39.4	SiO_2	44.4	42.9
TiO_2	2.61	2.76	TiO_2	1.84	2.06
Cr_2O_3	0.33	0.18	Al_2O_3	11.0	11.2
Al_2O_3	14.7	14.3	FeO[a]	6.89	7.17
FeO[a]	6.72	6.43	MnO	0.06	0.11
MgO	20.5	20.8	MgO	17.2	16.6
CaO	0.39	0.28	CaO	12.0	12.1
Na_2O	0.90	0.94	Na_2O	2.53	2.67
K_2O	8.86	9.38	K_2O	0.84	0.60
Cl	0.16	n.d.	Cl	0.26	0.07
Total	94.74	94.50	Total	96.98	95.37
xMg ($FeII^+$)	0.84	0.85	xMg ($FeII^+$)	0.82	0.81
Al (IV)	1.09	1.10	Al (IV)	1.56	1.66
Al (VI)	0.18	0.15	Al (VI)	0.32	0.29

[a]Total iron as FeO

Abbreviations: in: microinclusions inplagioclase (*pl*), clinopyroxene (*cpx*) and olivine (*ol*); *int*: interstitial; n.d.: not detected

Thermometric data were also obtained for the ultramafic xenoliths. The lack of orthopyroxene in the ultramafic samples does not allow the use of the two-pyroxene geothermometer of Köhler and Brey (1990). Similarly, the presence of phlogopite and amphibole (found in some gabbroic xenoliths) rules out the application of Loucks' geothermometer (Loucks 1996) for coexisting olivine and clinopyroxene (which is strictly applicable to nearly anhydrous or moderately hydrous assemblages, with $H_2O \leq 2$ wt%).

In this case, we applied several single-pyroxene geothermometers (such as Mercier 1980; Kretz 1982). The geothermometer of Kretz gives systematically higher temperatures. In particular, *wehrlites* have slightly higher equilibration temperatures (Table 11).

We then estimated temperatures by applying the geothermometer of Roeder et al. (1979) for the coexistence of olivine with Cr-spinel. The use of this geothermometer gave low temperatures (ranging between 700 and 930°C), likely due to thermal re-equilibration at depth (cf. Frost and Lindsley 1991). It is therefore likely that the ultramafic material experienced a significant cooling before being included into the uprising basaltic magmas.

Since no rhombohedrical phases have been found both in the xenoliths and the host lavas, we used the Fe_2O_3/FeO whole-rock values from Francalanci et al. (1993b), Hornig-Kjarsgaard et al. (1993) and retrieved oxygen fugacities over a range of temperatures by applying the algorithm of Kress and Carmichael (1991). These estimates indicate that Stromboli lavas plot along the Ni-NiO buffer of Hübner and Sato (1970), with only one sample being just slightly higher (i.e., within 1.2 log units). We will therefore use this buffer in calculating the pressure of equilibration of selected assemblages.

Table 8 Selected SEM-EDS analysis of glasses occurring in recent Strombolian lavas and associated mafic xenoliths

	Lavas								Gabbroic xenoliths				
Sample	St15	St15	St15	St15	St18	St21	St21	St21	St03	St03	St15	St13	St13
site	in (ol)	in (ol)	int	int	in (pl)	in (cpx)	in (pl)	in (cpx)	int	int	int	int	int
SiO_2	59.7	61.4	59.9	62.7	58.8	57.1	58.7	60.4	62.4	63.0	62.0	70.7	71.2
TiO_2	1.79	1.28	2.20	1.30	2.71	1.95	0.94	0.97	0.72	0.73	1.25	1.62	1.54
Al_2O_3	16.9	17.2	13.2	15.3	10.9	14.0	16.3	16.8	19.3	19.5	19.2	12.9	15.9
FeO[a]	4.70	4.16	6.97	5.32	7.04	11.21	5.85	6.02	2.98	3.01	2.90	2.92	1.62
MnO	0.20	0.06	0.11	n.d.	0.16	0.38	0.25	0.26	0.51	0.51	0.26	0.15	n.d.
MgO	1.20	1.24	1.93	1.14	3.72	3.77	2.48	2.56	0.56	0.57	0.85	1.22	0.26
CaO	5.77	6.45	3.91	6.47	6.03	6.94	7.22	7.43	2.97	3.00	4.80	1.51	1.20
Na_2O	3.31	3.48	3.29	2.96	1.98	2.35	3.02	3.11	3.64	3.68	4.60	2.24	2.55
K_2O	4.40	4.01	5.35	4.62	3.82	2.11	2.17	2.23	5.87	5.93	4.12	5.30	5.67
P_2O_5	0.82	n.d.	1.10	n.d.	0.31	n.d.	n.d.	n.d.	n.d.	n.d.	n.d.	n.d.	n.d.
Total	98.77	99.25	97.89	99.80	95.38	99.79	96.94	99.80	98.91	99.90	99.91	98.50	99.89
Mg#	0.31	0.35	0.33	0.28	0.48	0.37	0.43	0.43	0.25	0.25	0.34	0.43	0.22

[a]Total iron as FeO

Abbreviations: in: microinclusions in plagioclase (*pl*), clinopyroxene (*cpx*) and olivine (*ol*); *int*: interstitial; n.d.: not detected

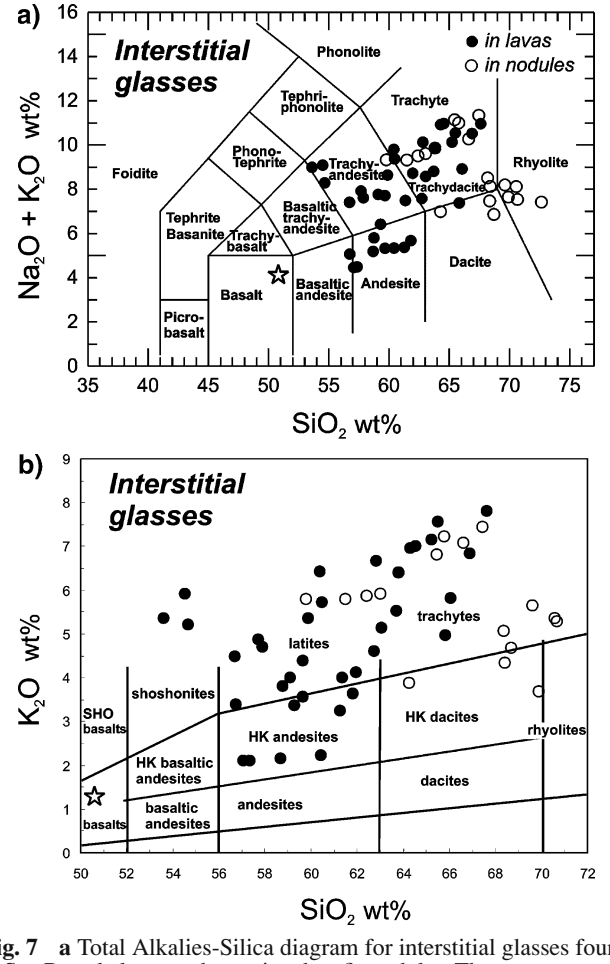

Fig. 7 **a** Total Alkalies-Silica diagram for interstitial glasses found in San Bartolo lavas and associated mafic nodules. The star represents the bulk composition of San Bartolo lavas; **b** K_2O vs. SiO_2 diagram of Peccerillo and Taylor (1976) for the interstitial glasses of San Bartolo lavas and associated mafic nodules. The *star* is the bulk composition of San Bartolo lavas

Geobarometry

In order to constrain the P-T regimes associated with the crystallization of lava phenocrysts and gabbroic xenoliths we constructed a grid of reactions representative of the equilibrium assemblages. This approach is particularly helpful in decoding the depth of interactions between the mafic and ultramafic materials with the uprising magmas since the thermobarometer of Mercier (1980) gave excessively high pressures of equilibration for the wherlitic assemblages. Reactions that satisfy our search for equilibrium conditions are the following:

$$\underset{\text{An}}{CaAl_2Si_2O_8} = \underset{\text{CaTs}}{CaAl_2SiO_6} + \underset{\text{liq}}{SiO_2} \quad (1)$$

$$\underset{\text{An}}{CaAl_2Si_2O_8} + \underset{\text{Fo}}{2Mg_2SiO_4} + \underset{\text{liq}}{SiO_2} = \underset{\text{CEn}}{2Mg_2Si_2O_6} + \underset{\text{CaTs}}{CaAl_2SiO_6} \quad (2)$$

$$\underset{\text{An}}{CaAl_2Si_2O_8} + \underset{\text{Fo}}{2Mg_2SiO_4} + \underset{\text{liq}}{SiO_2} = \underset{\text{OEn}}{2Mg_2Si_2O_6} + \underset{\text{CaTs}}{CaAl_2SiO_6} \quad (3)$$

$$\underset{\text{Di}}{CaMgSi_2O_6} = \underset{\text{liq}}{1/2\,SiO_2} + \underset{\text{Fo(sol)}}{1/2\,Mg_2SiO_4} + \underset{\text{Wo(liq)}}{Ca_2Si_2O_6} \quad (4)$$

$$\underset{\text{Fo(sol)}}{Mg_2SiO_4} = \underset{\text{Fo(liq)}}{Mg_2SiO_4} \quad (5)$$

Table 9 Representative whole rocks chemical analysis (major and trace elements) of host lavas, mafic and ultramafic xenoliths included in S. Bartolo lavas

	Lavas				Gabbros			Ultramafics		
Sample	Str1	Str2	Str37	Str38	Str15	Str4	Str22	Str7	Str21	Str36
Type	S. Bartolo Lava	S. Bartolo Lava	Lava 1975	Lava 1985	gabbroanorthosite	gabbro	gabbro	dunite	wherlite	clinopyroxenite
SiO_2	51.13	51.20	49.32	49.43	45.80	49.95	48.47	40.40	44.85	54.14
TiO_2	0.76	0.76	0.88	0.90	0.24	0.88	0.59	0.11	0.25	0.11
Al_2O_3	16.91	16.97	16.47	16.39	21.73	15.64	12.45	0.52	3.63	1.12
Fe_2O_3[a]	8.09	8.05	8.60	8.56	5.61	6.14	8.22	9.92	11.71	4.34
MnO	0.14	0.14	0.15	0.15	0.09	0.13	0.28	0.14	0.19	0.07
MgO	7.25	7.28	7.08	7.12	8.66	7.79	9.29	47.82	28.61	17.88
CaO	10.62	10.61	11.38	11.47	15.75	15.16	15.37	0.36	9.17	21.16
Na_2O	2.28	2.29	2.49	2.42	0.87	2.02	1.87	0.08	0.43	0.19
K_2O	1.76	1.71	1.97	2.34	0.42	0.32	0.39	0.11	0.24	0.20
P_2O_5	0.23	0.24	0.46	0.49	0.03	0.49	0.17	0.1	0.14	0.08
LOI	0.40	0.30	0.80	0.30	0.60	1.00	2.10	0.02	0.05	0.04
Total	99.57	99.55	99.60	99.57	99.85	99.61	99.33	99.58	99.27	99.33
V	235	231	246	245	101	290	217	131.8	126.6	n.d.
Cr	98	98	84	107	615.9	307.9	130.0	672.9	810.0	1355.5
Co	35	33	36	31.8	65	86.4	470.4	101.47	109.8	33.6
Ni	65	67	53	47	87	76	126	546.2	596.4	154.7
Cu	23	24	86	81	49	43	85	18.87	22.17	22.8
Zn	32	31	42	37	27	13	47	66.47	78.89	40.6
Ga	17.4	17.1	16.9	16.2	13.9	19.6	13.4	3.83	4.27	n.d.
Rb	64	62	66.3	69.3	10.7	5.2	8.1	5.08	9.09	1.9
Sr	542.2	526	763.5	774.3	645.9	698.7	604.8	61.5	89.5	50.9
Y	23	22	26.3	27.5	8	33.2	18.7	4.93	6.9	11.1
Zr	104.4	102.2	142.8	150.3	23	125.4	53.7	18.48	24.92	45.8
Nb	11.6	11.7	20.2	21.3	1.4	12.3	8.4	1.58	1.93	0.7
Mo	1.1	1.1	1.6	1.5	0.7	1.3	6.9	1.78	n.d.	0.4
Cd	0.2	0.2	0.2	0.2	0.2	0.2	0.2	0.04	n.d.	n.d.
Sn	3	2	2	2	1	2	1	0.27	0.71	36.4
Cs	3.7	3.7	2.4	2.3	0.6	0.3	0.4	0.43	0.64	0.18
Ba	734	733	1014	1088	173	284	124	79.07	120.2	16.5
Hf	2.4	2.3	3.5	3.4	0.7	3.2	1.7	0.46	0.67	1.40
Ta	1.6	1.6	1.4	1	1.0	1.3	3.5	0.12	0.13	0.05
Pb	2	2	4	4	2	2	4	1.63	3.50	4.33
Bi	0.5	0.5	0.5	0.5	0.5	0.5	0.5	0.0	n.d.	n.d.
Th	12.1	11.6	14.3	15.7	2.4	9.2	3.6	1.37	1.92	0.88
U	3.3	3.1	3.9	4.5	0.5	2.5	1.8	0.323	0.5	0.31
Sc	31	31	32	32	29	36	45	7.88	n.d.	75.6

[a]Total iron as Fe_2O_3

Abbreviations: n.d., not detected; n.a.: not analyzed

$$\underset{\text{An}}{CaAl_2Si_2O_8} + \underset{\text{Fo}}{Mg_2SiO_4} = \underset{\text{CEn}}{Mg_2Si_2O_6} + \underset{\text{CaTs}}{CaAl_2SiO_6} \quad (6)$$

$$\underset{\text{An}}{CaAl_2Si_2O_8} + \underset{\text{Fo}}{Mg_2SiO_4} = \underset{\text{OEn}}{Mg_2Si_2O_6} + \underset{\text{CaTs}}{CaAl_2SiO_6} \quad (7)$$

$$\underset{\text{Fo}}{Mg_2SiO_4} + \underset{\text{liq}}{SiO_2} = \underset{\text{CEn}}{Mg_2Si_2O_6} \quad (8)$$

The first five have been used to estimate P-T regimes associated with the crystallization of the lavas (Fig. 10), whereas the pressure of crystallization of the gabbroic xenoliths has been estimated by means of reactions (6) and (7) in the light of previously discussed geothermometric data (cf. Table 11). Other heterogeneous equilibria (i.e., those involving solid and liquid phases) are thought to define the temperature and pressure of interactions between the uprising magma and the host "xenoliths", either mafic

Table 10 Representative REE analyses for mafic and ultramafic xenoliths included in S. Bartolo lava field and host lavas

	Lavas				Gabbros			Ultramafics		
Sample	Str1	Str2	Str37	Str38	Str15	Str4	Str22	Str7	Str21	Str36
Type	S. Bartolo Lava	S. Bartolo Lava	Lava 1975	Lava 1985	gabbroanorthosite	gabbro	gabbro	dunite	wherlite	clinopyroxenite
La	32.9	31.0	50.3	52.1	8.2	64.4	28.6	3.99	5.38	6.33
Ce	53.9	51.0	84.6	88.9	15.6	101.4	48.3	8.49	12.1	12.3
Pr	6.39	6.01	10.4	11	1.77	12.1	5.81	0.98	1.54	1.80
Nd	24.6	24.4	40.3	41	7.6	43.8	22.5	3.75	6.38	8.08
Sm	5.1	4.8	7.9	8.6	1.8	7.9	4.5	0.79	1.60	2.25
Eu	1.40	1.40	2.18	2.27	0.65	2.04	1.27	0.22	0.43	0.55
Gd	4.51	4.74	6.91	6.76	1.62	6.73	4.12	0.75	1.47	2.00
Tb	0.7	0.7	0.9	1.0	0.3	0.6	1.0	0.12	0.22	0.32
Dy	3.69	3.58	5.17	5.26	1.36	5.40	3.43	0.75	1.25	2.17
Ho	0.74	0.74	0.87	0.98	0.29	1.0	0.68	0.15	0.23	0.40
Er	2.02	2.08	2.38	2.38	0.72	2.62	1.68	0.44	0.61	1.06
Tm	0.29	0.30	0.37	0.37	0.10	0.39	0.25	0.06	0.09	0.15
Yb	1.98	1.96	2.02	2.36	0.61	2.55	1.79	0.42	0.59	1.04
Lu	0.30	0.31	0.34	0.35	0.09	0.40	0.26	0.07	0.09	0.21

Abbreviations: n.d., not detected

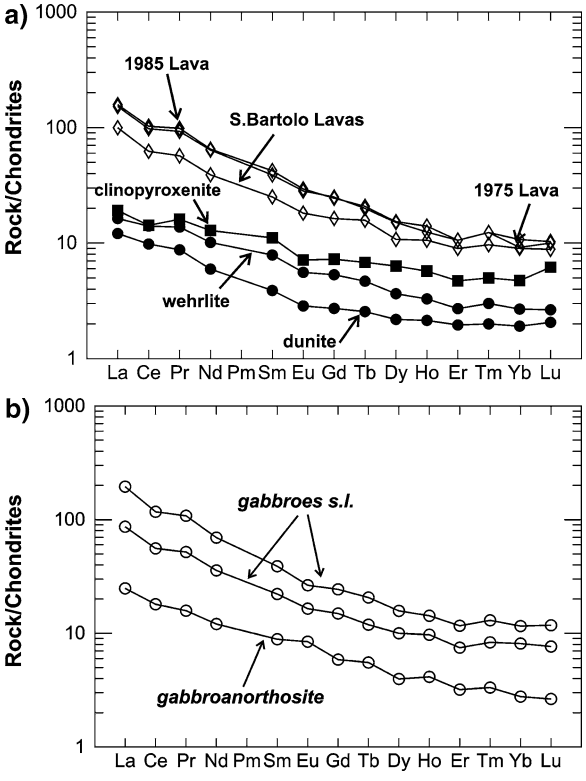

Fig. 8 **a** Chondrite-normalized REE patterns (according to Nakamura 1974) for recent lavas and associated ultramafic xenoliths (the latter were only found in S.Bartolo lavas; **b** Chondrite-normalized REE patterns (Nakamura 1974) for mafic xenoliths found in S. Bartolo lavas

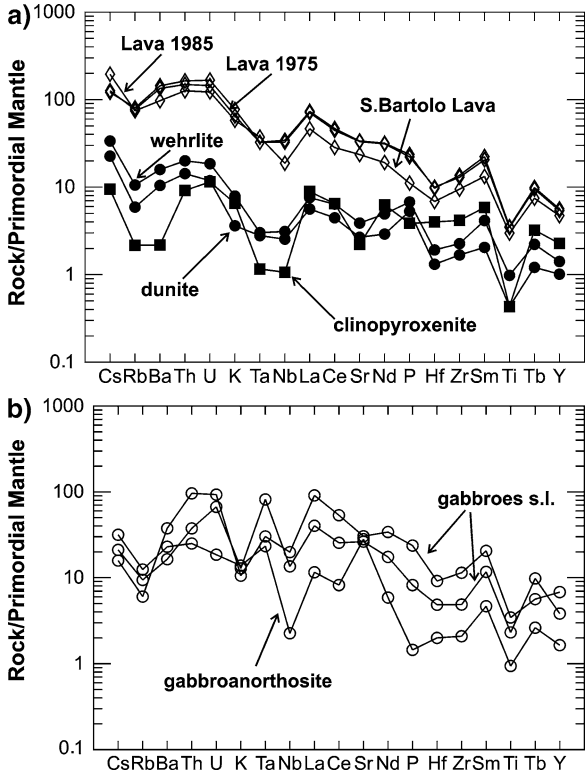

Fig. 9 **a** Spider diagrams for recent lavas and associated ultramafic xenoliths. **b** Spider diagram for mafic xenoliths found in S. Bartolo lavas. Trace elements abundances were normalized to primordial mantle values (according to Wood et al. 1979)

or ultramafic (Fig. 11). In these calculations we used the San Bartolo HKCA basaltic lavas as the melt phase, being in equilibrium with its own mineral phases or "host gabbroic and ultramafic" materials.

Gibbs free energies, volume expansions and compressibility have been calculated by using the thermodynamic data of Berman (1988; Table 2 and Table 3, and Table 4, p. 458–469) on plagioclase and ferromagnesian phases, together with those of Richet et al. (1982) for amorphous

Table 11 Summary of thermometric estimates for recent Stromboli lavas and associated xenoliths (see text for details)

Samples	T range (°C)	Geothermometers
S. Bartolo lavas	1060–1130	(a)
gabbroic xenoliths	940–1030	(a)
dunites	890–1000	(b)
wherlites	740–930	(b)
wherlites	970–1080	(c)
wherlites	1060–1170	(d)

(a) QUILF (Andersen et al. 1993): reaction Di(Cpx)=Di(Opx) is the one that better satisfy free energy minimization criteria imposed by the program; (b) Roeder et al.; (c) Mercier (1980); (d) Kretz (1982)

silica, and those of Ghiorso and Sack (1995) for other melt components (a synopsis of the latter data is given by Ghiorso and Sack 1995; Table A1, p. 209).

Activity models, both for solid and melt components, used in calculations are summarized for S. Bartolo lavas and related xenoliths in Table 12. As previously mentioned, we estimated that the magma had an oxygen fugacity on the Ni-NiO buffer defined by Hübner and Sato (1970). Therefore we calculated the degree of oxidation of the melt (which is sensitive to pressure and temperature variations) by using the algorithm of Kress and Carmichael (1991) for the above buffer. Water contents in the melt were calculated by using the method of Sisson and Grove (1993), which has been experimentally determined for calc-alkaline magmas. According to this algorithm, the water content is temperature, pressure and compositionally dependent but, at high temperatures (approaching 1,200°C), will tend toward anhydrous conditions (cf. pp. 178–179 of their work). Therefore, calculations involving *hydrous melt components* are more reliable at lower temperatures. Since, at higher pressure solid-melt interactions are assumed to occur at higher temperatures, we could not use this algorithm for estimating interactions between the basaltic magma and the ultramafic xenoliths. In this case, we assumed that the basalt had about 3 wt% of H_2O as we found relict amphibole and phlogopite in some of our gabbroic inclusions. This water content is slightly higher than the minimum water content for the crystallization of amphibole within a high-alumina basalt (cf. the experimental data of Foden and Green 1992).

Graphic solutions for reactions (2) and (4) plotted on a P-T diagram further constrain temperature and pressure of equilibration to 1,140–1,170°C and 0.72 to 0.8 GPa for the *"hydrous" basaltic magmas* (San Bartolo lavas) with olivine (Fo_{80}), as a stable phase. Estimated water contents range from about 1.6 to 2.8 wt%. Anhydrous assemblages result in unrealistically high temperatures and nearly identical pressures of equilibration (Figs. 10, 11). However, solutions for *hydrous olivine-orthopyroxene-plagioclase-melt* assemblages, given by reactions (1), (3) and (4), define a lower a temperature and pressure, being approximately 1,060°C and 0.32 GPa where the three curves converge (Fig. 10). In this case water contents were calculated to be around 4.5 wt%. Graphic solutions given by reactions (1), (3) and (4) for such a similar but *anhydrous assemblage*

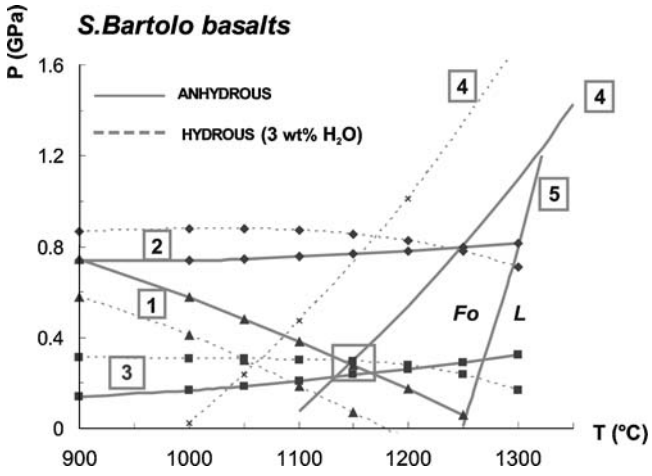

Fig. 10 Summary of thermobarometric estimates for S. Bartolo lava. Calculations have been performed for selected reactions (shown with numbers consistent with those reported in the text) by solving thermodynamic solid-melt equilibria both for hydrous and anhydrous conditions. The best solution (0.27 GPa and 1,160°C) is given by the intersections of reactions (1), (3) and (4) identified by the unnumbered rectangle (see text). Activity models used in calculations are the following: olivine and orthopyroxene: Sack and Ghiorso (1989); clinopyroxene: Gasparik (1984); plagioclase: Newton et al. (1980); melt components: Ghiorso and Sack (1995). See text and Table 12 for details

(which involves both clinopyroxene and orthopyroxene) give a pressure of about 0.27 GPa and a temperature of 1,160°C (Fig. 10). These estimates seem to be more reliable since olivine is stable at relatively low pressures within a calc-alkaline basalt and coexists with orthopyroxene, as suggested by Baker and Eggler (1987). In this case we assumed an olivine composition of Fo_{73} in agreement with the average content of olivines found S. Bartolo lavas (cf. Fig. 5). As shown by the same Authors, clinopyroxene is fractionating with a Ca-rich plagioclase at higher pressures: i.e., during the early stages of evolution of a calc-alkaline basaltic melt.

Thermobarometric estimates for the *crystallization* of *gabbroic xenoliths* derived from reactions (6) and (7) without the involvement of a melt phase (Fig. 11). Also in this case the equilibration pressures for the *orthopyroxene-bearing assemblage* (reaction 7) gives lower pressures, ranging from 0.24 to 0.17 GPa for temperatures of 940–1,030°C (obtained by using the two-pyroxene geothermometer, Table 11. For similar temperatures, reaction (6) shows that clinopyroxene-bearing assemblages equilibrate at slightly higher pressures, being 0.35 to 0.42 GPa, respectively. We therefore regard these regimes as the upper pressure limit for the crystallization of the gabbroic materials.

However, graphic solutions reported in Fig. 11 are representative of the P-T regimes of *interactions* between the gabbroic materials and the uprising basaltic magmas. Under hydrous conditions, such interactions occur in the subvolcanic region at pressures of ~0.46 GPa at temperatures of about 1,070°C. Anhydrous magmas, with temperatures ranging from 1,100 to 1,150°C, are estimated to have equilibrated with gabbroic materials at slightly lower pressures

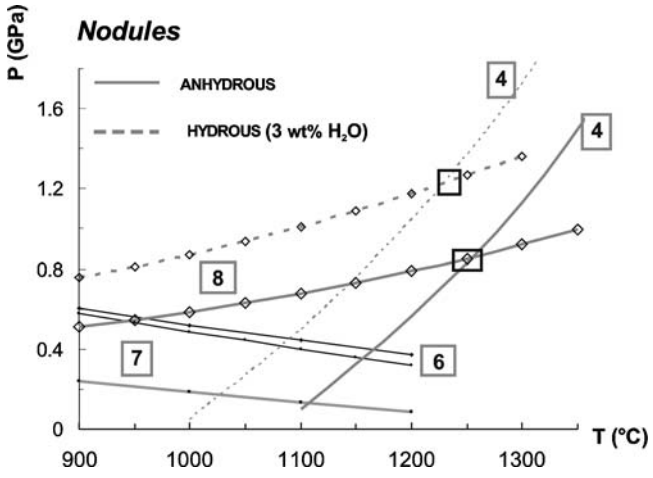

Fig. 11 Summary of thermobarometric estimates for mafic and ultramafic xenoliths in equilibrium with San Bartolo basalt. Calculations for a hydrous melt phase were performed at a fixed water content (3 wt%, see text). Barometric estimates for the mafic-xenolithic assemblages are given by reactions (6) and (7) consistent the geothermometric data reported in Table 11. Best estimates are 0.17–0.38 GPa for temperatures ranging 1,100–1,150°C under anhydrous conditions, whereas under hydrous conditions reach a pressure of ∼0.46 GPa at T∼1,070 °C. Representative solutions for the ultramafic assemblage in equilibrium with the basaltic melt are given by the intersections of reactions (8) and (4), both under hydrous and anhydrous conditions, and are identified by the unnumbered rectangles. See text and Table 12 for details

(0.17–0.38 GPa). Our calculations suggest that within an "open conduit" volcano, such as Stromboli, magma masses may start degassing at greater depth and reach the surface approaching anhydrous conditions before erupting.

Finally, thermobarometric estimates have been obtained for the interaction of the ultramafic xenoliths with Strombolian basaltic magmas (Fig. 11). For a *hydrous basaltic melt* (with 3 wt% of H_2O) coexisting with wherlitic materials, equilibration conditions are reached at about 1.2 GPa and temperatures approaching 1,240°C. By increasing the water content up to 4 wt%, this equilibrium is shifted to a higher pressure (up to about 1.35 GPa). Under anhydrous conditions, the wherlitic assemblage could have equilibrated with the basaltic melt at lower pressures (i.e., 0.82 GPa) and slightly higher temperatures (up to 1,280°C).

Discussion

The main task of this work is to characterize the textural and petrochemical features of mafic and ultramafic nodules and to estimate the P-T regimes where interactions between uprising basaltic magma and cumulitic materials (eventually "recycled") are likely to occur. We will also discuss some petrogenetic features of Stromboli magmas in order to offer a guideline for future research.

The petrographic and petrochemical data presented in this contribution indicate a close genetic link for the gabbroic and ultramafic nodules and the high-K calc-alkaline to shoshonitic lavas recently erupted. In particular, San Bartolo lavas contain abundant crystal clots and xenocrysts related to the disaggregation of mafic and ultramafic materials. Gabbroic nodules equilibrated with HKCA basaltic magmas (hydrous and/or anhydrous) at pressures ranging 0.17 to 0.46 GPa and temperatures of 1,050–1,150°C. Similar conditions are also obtained for the crystallization of the phenocrystic phases of the basaltic lava. Therefore, gabbroic inclusions are interpreted as cumulates which represent crystallized portions of earlier Stromboli-type basalts that, in turn, were stored in the subvolcanic region before being erupted. Our calculations show that San Bartolo basalts reach a temperature of 1,100–1,150°C in the subvolcanic region (i.e., at about 0.3 GPa pressure) for water contents of about 3.5 and 2 wt% and may degas undergoing a moderate decompression (to about 0.2 GPa), before being erupted at nearly anhydrous conditions (cf. Table 12). However, Métrich et al. (2001), and Bertagnini et al. (2003) measured similar water contents for the melt inclusions found within the olivine of the basaltic *pumices* and *scoriae* ejected during the major explosive eruption of August 1998, and estimated nearly identical P-T ranges (by using the solubility model of Papale 1999). Therefore, the difference in the eruptive styles (i.e., effusive vs. explosive) seems to be related to the residence time of the magma batches in the subvolcanic region. In other words the longer a magma batch is stored in the subvolcanic region, the more this magma will undergo diffuse degassing (through the fracture networks and the hydrothermal system), as indicated by short-lived isotope data (Gauthier and Condomines 1999).

We may therefore conclude that during large effusive eruptions (such as the one of San Bartolo lava field) Stromboli magmas may reach the surface approaching anhydrous conditions (i.e., after substantial degassing at depth), whereas the eruption of *pumices* is related to the rapid uprise of an undegassed magma batch undergoing fragmentation within an open conduit (e.g., Klug and Cashman 1996).

Ultramafic "xenoliths" also reflect comagmatism with Strombolian basaltic lavas and they interacted with ascending magmas at pressures of 0.8–1.2 GPa (∼24–36 km depth), thus corresponding to greater depths than the crust-mantle transition under Stromboli volcano (cf. Morelli et al. 1975; Panza and Pontevivo 2002). These Authors identified a sharp decrease in S-wave velocities at about 15–18 km depth, followed by a definite and constant increase at about 32 km depth. Therefore the source region of Stromboli parental magmas will reside deeper into the mantle as shown by the concentration of earthquakes' hypocenters below Stromboli volcano (cf. Panza and Pontevivo 2002).

Thermobarometric data suggests that the plumbing system of Stromboli is characterized by a by a deep "root zone" above which basaltic magmas are stored and partly crystallize (at about 24–36 km depth) before migrating to upper crustal levels. This lower magma chamber seems to be connected, likely through a feeder dike, to an upper reservoir located between 4.5 and 15 km below the volcano. The upper part of this plumbing system seems to be rather similar to that found at Arenal, where similar gab-

Table 12 Summary of selected thermodynamic solutions for solid-liquid equilibria for S. Bartolo lavas and related xenoliths. Melt components have been calculated by means of analysis n. 1, Table 9. Solutions for gabbroic and wehrlitic xenoliths are thought to represent the P-T regimes of interactions of these materials with an ascending basaltic melt having the composition of S. Bartolo lavas. Water content where not indicated is calculated with the method of Sisson and Grove (1993) for a calc-alkaline magma, exception of the wehrlitic assemblage in equilibrium with the San Bartolo basalt (containing 3 wt% of H_2O). See text for details

Reaction (3)[a]								An+2Fo+SiO_2=2OEn+Cats		
T°C	a_{An}	a_{Fo}	a_{OEn}	a_{Cats}	log a_{SiO_2} anhydrous	log a_{SiO_2} hydrous	% H_2O	P (GPa) anhydrous	P (GPa) hydrous	
S. Bartolo lava										
1000	0.505	0.692	0.505	0.050	−0.380	−0.503	6.4	0.20	0.32	
1100	0.497	0.680	0.497	0.049	−0.377	−0.464	3.5	0.23	0.32	
1150	0.494	0.673	0.494	0.048	−0.376	−0.432	1.9	0.23	0.30	
1200	0.491	0.666	0.491	0.048	−0.375	−0.389	0.4	0.27	0.28	
1250	0.489	0.660	0.489	0.047	−0.373	−0.329	–	0.30	0.30	
1300	0.486	0.655	0.487	0.047	−0.372	−0.244	–	0.32	0.32	
model	asymmetric ss	asymmetric ss	asymmetric ss	Redlich-Kister eq.	regular solution	regular solution				
reference	Newton et al. (1980)	Sack and Ghiorso (1989)	Sack and Ghiorso (1989)	Gasparik (1984)	Ghiorso and Sack (1995)	Ghiorso and Sack (1995)	Sisson & Grove (1993)			
Reaction (7) & (3)[b]								An+2Fo+SiO_2=2OEn+Cats		An+Fo=Cats+OEn
T°C	a_{An}	a_{Fo}	a_{OEn}	a_{Cats}	log a_{SiO_2} anhydrous	log a_{SiO_2} hydrous	% H_2O	P (GPa) anhydrous	P (GPa) hydrous	P_{total} (GPa)
Gabbros										
900	0.596	0.750	0.608	0.044	−0.369	−0.504	9.4	0.13	0.24	0.24
950	0.594	0.744	0.594	0.043	−0.368	−0.499	7.9	0.13	0.25	0.21
1000	0.591	0.739	0.603	0.043	−0.366	−0.489	6.4	0.16	0.26	0.18
1050	0.589	0.735	0.589	0.042	−0.365	−0.473	4.9	0.16	0.27	0.16
1100	0.587	0.730	0.599	0.041	−0.364	−0.449	3.5	0.19	0.26	0.13
1150	0.586	0.726	0.543	0.041	−0.363	−0.428	1.9	0.21	0.25	0.12
1200	0.583	0.723	0.595	0.040	−0.362	−0.371	0.4	0.24	0.24	0.09
model	asymmetric ss	asymmetric ss	asymmetric ss	Redlich-Kister eq	regular solution	regular solution				
reference	Newton et al. (1980)	Sack and Ghiorso (1989)	Sack and Ghiorso (1989)	Gasparik (1984, 1990)	Ghiorso and Sack (1995)	Ghiorso and Sack (1995)	Sisson & Grove (1993)			
Reaction (8)[c]						Fo (sol)+SiO_2=CEn				
T°C	a_{Fo}	a_{En}	log $a^*_{Sio_2}$ anhydrous	log $a^*_{Sio_2}$ hydrous	% H_2O	P (GPa) anhydrous	P (GPa) anhydrous			
Wherlite										
900	0.744	0.5975	−0.396	−0.474	3	0.51	0.76			
1000	0.733	0.5979	−0.397	−0.477	3	0.58	0.87			
1100	0.723	0.5982	−0.399	−0.479	3	0.68	1.13			
1200	0.714	0.6120	−0.397	−0.477	3	0.79	1.76			
1300	0.707	0.6124	−0.399	−0.479	3	0.92	1.61			
model	asymmetric ss	asymmetric ss	regular solution	regular solution						
reference	Sack and Ghiorso (1989)	Sack and Ghiorso (1989)	Ghiorso and Sack (1995)	Ghiorso and Sack (1995)						

[a] X_{An}=0.8, X_{Fo}=0.73, X_{OEn}=0.7; a_{CaTs} calculated for clinopyroxene an. 1, Table 4

[b] X_{An}=0.9, X_{Fo}=0.79, X_{OEn}=0.73; a_{CaTs} calculated for clinopyroxene an. 12, Table 4

[c] X_{Fo}=0.83; a_{CaTs} calculated for clinopyroxene an. 18, Table 4

broic and anorthositic inclusions have been found (Cigolini and Kudo 1987; Cigolini 1998).

In particular, the style of eruption associated with the emplacement of San Bartolo lava field was very different from the present-day activity as suggested by Rosi et al. (2000). These differences may reflect important changes in the geometry and dynamics of the plumbing system (likely between the III and VII century AD according to Rosi et al. 2000) since San Bartolo basalts have undergone substantial degassing before eruption. These changes seems to be also associated with variations in the chemical composition of the erupted materials (from HKCA to HKCA-SHO), as previously outlined by several Authors (e.g., Francalanci et al. 1989, 1993b; Hornig-Kjarsgaard et al. 1993; Rosi et al. 2000).

Acknowledgments Financial support has been provided by INGV-GNV as part of the coordinated project "Eruptive Scenarios from Physical Modeling and Experimental Volcanology". Additional support has been provided by the Italian Ministry for Universities and Research (MIUR). Thanks to A. Peccerillo, L. Francalanci an N. Métrich for their helpful comments during the IAVCEI Meeting "Montagne Pelée", held in Saint Pierre, Martinique. R. Ruffini provided valued assistance during the analythical work. The National Volcanology Group of Italy (GNV) offered logistic support during the stay of one of us (M. Laiolo) at Stromboli. C. Hawkesworth, S. Conticelli, P. Landi, R. Cioni and H.G. Stosch provided a constructive review of an earlier draft of the paper. L. Wesely revised the English.

References

Allard P, Carbonelle J, Métrich N, Loyer H, Zettwoog P (1994) Sulphur output and magma degassing budget of Stromboli volcano. Nature 368:326–340

Andersen DJ, Lindsley DH, Davidson PM (1993) QUILF: a Pascal program to assess equilibria among Fe-Mg-Mn-Ti oxides, pyroxenes, olivine and quartz. Comput Geosci 19(9):1333–1350

Baker DR, Eggler DH (1987) Compositions of anhydrous and hydrous melts coexisting with plagioclase, augite, and olivine of low-Ca pyroxene from 1 atm to 8 kbar: application to Aleutian volcanic center of Atka. Am Mineral 72:12–28

Barberi F, Innocenti F, Ferrara G, Keller J, Villari L (1974) Evolution of Eolian Arc volcanism (Southern Tyrrhenian Sea). Earth Planet Sci Lett 21:269–276

Barberi F, Rosi M, Sodi A (1993) Volcanic hazard assessment at Stromboli based on review of historical data. Acta Vulcanol 3:173–187

Beard JS, Borgia A (1989) Temporal variation of mineralogy and petrology in cognate gabbroic enclaves at Arenal Volcano, Costa Rica. Contrib Mineral Petrol 103:110–122

Berman RG (1988) Internally consistent thermodynamic data for stoichiometric minerals in the system Na_2O-K_2O-CaO-MgO-FeO-Fe_2O_3-Al_2O_3-SiO_2-TiO_2-H_2O-CO_2. J Petrol 29:445–522

Bertagnini A, Coltelli M, Landi P, Pompilio M, Rosi M (1999) Violent explosions yield new insights into dynamics of Stromboli volcano. Eos Trans AGU 80(52):633–636

Bertagnini A, Métrich N, Landi P, Rosi M (2003) Stromboli volcano (Aeolian Archipelago, Italy): an open window on the deep-feeding system of a steady state basaltic volcano. J Geophys Res 108/B7:3336

Bonaccorso A, Cardaci C, Coltelli M, Del Carlo P, Falsaperla S, Panucci S, Pompilio M, Villari L (1996) Annual report of the world volcanic eruptions in 1993, Stromboli. Suppl Bull Volcanic Eruptions 35:8–14

Cabanes N, Mercier JCC (1988) Insight into the upper mantle beneath an active extensional zone: spinel-peridotite xenoliths from San Quintin (Baja California, Mexico). Contrib Mineral Petrol 100:374–382

Calanchi N, Peccerillo A, Tranne CA, Lucchini F, Rossi PL, Kempton P, Barbieri M, Wu TW (2002) Petrology and geochemistry of volcanic rocks from the island of Panarea: implications for mantle evolution beneath the Aeolian island arc (southern Tyrrhenian sea). J Volcanol Geotherm Res 115(3-4):367–395

Capaldi G, Guerra I, Lo Bascio A, Pece R, Rapolla A, Scarpa R, Del Pezzo E, Martini M, Ghiara MR, Lirer L, Munno R, La Volpe L (1978) Stromboli and its 1975 eruption. Bull Volcanol 43–1:259–285

Cigolini C, Kudo AM (1987) Xenoliths in recent basaltic andesite flows from Arenal Volcano, Costa Rica: inference on the composition of the lower crust. Contrib Mineral Petrol 96:381–390

Cigolini C (1998) Intracrustal origin of Arenal basaltic andesite in the light of solid-melt interactions and related compositional buffering. J Volcanol Geotherm Res 86:277–310

Coltelli M, Falsaperla S, Del Carlo P, Pompilio M, Bonaccorso A (1999) Volcanic, seismic, and ground deformation data concerning the Stromboli volcano in 1995. Suppl Bull Volcanic Eruptions 35:8–14

Conticelli S, Peccerillo A (1990) Petrological significance of high-pressure ultramafic xenoliths from ultrapotassic rocks of Central Italy. Lithos 24:305–322

De Astis G, LaVolpe L, Peccerillo A, Civetta L (1997) Volcanological and petrological evolution of Vulcano Island (Aeolian arc, southern Tyrrhenian Sea). J Geophys Res—Sol Earth 102:8021–8050

De Fino M, La Volpe L, Falsaperla S, Franzetta G, Neri G, Francalanci L, Rosi M, Sbrana A (1988) The Stromboli eruption of December 6, 1985–April 25, 1986: volcanological, petrochemical and seismological data. Rend Soc It Miner Petrol 43:1021–1038

Dickinson WR (1968) Circum-pacific Andesite type. J Geoph Res 73:2261–2269

Ellam RM, Hawkesworth CJ, Menzies MA, Rogers NW (1989) The Volcanism of Southern Italy: Role of Subduction and the Relationship between Potassic and Sodic Alkaline Magmatism. J Geoph Res 94:4589–4601

Ernst WG (1978) Petrochemical study of some lherzolitic rocks from the Western Alps. J Petrol 19:341–392

Ernst WG, Piccardo GB (1979) Petrogenesis of some ligurian peridotites–I Mineral and bulk-rock chemistry. Geochim Cosmochim Acta 43:219–237

Finizola A, Sortino F, Lenat JF, Valenza M (2002) Fluid circulation at Stromboli volcano (Aeolian Islands, Italy) from self-potential and CO_2 surveys. J Volcanol Geoth Res 116:1–18

Foden JD, Green DH (1992) Possible role of amphibole in the origin of andesite: some experimental and natural evidence. Contrib Mineral Petrol 109:479–493

Francalanci L, Manetti P, Peccerillo A (1989) Volcanological and magmatological evolution of Stromboli volcano (Aeolian Islands): the roles of fractional crystallisation, magma mixing, crustal contamination and source heterogeneity. Bull Volcanol 51:355–378

Francalanci L, Manetti P, Peccerillo A, Keller J (1993a) Magmatological evolution of the Stromboli volcano (Aeolian Arc, Italy): inferences from major and trace element and Sr isotopic composition of lavas and pyroclastic rocks. Acta Vulcanol 3:127–151

Francalanci L, Taylor SR, McCulloch MT, Woodhead JD (1993b) Geochemical and isotopic variations in the calc-alkaline rocks of Aeolian arc, southern Tyrrhenian Sea, Italy: constraints on magma genesis. Contr Mineral Petrol 113:300–313

Francalanci L, Tommasini S, Conticelli S, Davies GR (1999) Sr isotope evidence for short magma residence time for the 20th century activity at Stromboli volcano, Italy. Earth Planet Sci Lett 167:61–69

Francalanci L, Tommasini S, Conticelli S (2004) The volcanic activity of Stromboli in the 1906–1998 AD period: mineralogical, geochemical and isotope data relevant to the understanding of the plumbing system. J Volcanol Geoth Res 131:179–211

Frost BR, Lindsley DH (1991) Occurrence of iron-titanium oxides in igneous rocks. In: Lindsley DH (ed), Oxide minerals: petrologic and magmatic significance. Rev Miner Mineral Soc Am 25:433–468

Gardner PM, Robins B (1974) The olivine-plagioclase reaction: geological evidence from the Seiland petrographic province, northern Norway. Contrib Mineral Petrol 44:149–156

Gasparik T (1984) Two pyroxene thermobarometry with new experimental data in the CaO-MgO-Al_2O_3-SiO_2. Contrib Mineral Petrol 87:87–97

Gauthier PJ, Condomines M (1999) ^{210}Pb-^{226}Ra radioactive disequilibria in recent lavas and radon degassing: inferences on the magma chamber dynamics at Stromboli and Merapi volcanoes. J Volcanol Geothermal Res 172:111–126

Ghiorso MS, Sack RO (1995) Chemical mass transfer in magmatic processes: IV A revised and internally consistent thermodynamic model for the interpolation and extrapolation of liquid-solid equilibria in magmatic systems at elevated temperature and pressures. Contrib Mineral Petrol 119:197–212

Gillot PY, Keller J (1993) Radiochronological dating of Stromboli. Acta Vulcanol 3:69–77

Hornig-Kjarsgaard I, Keller J, Koberski U, Stadbauer E, Francalanci L, Lenhart R (1993) Geology, stratigraphy and volcanological evolution of the island of Stromboli, Aeolian arc, Italy. Acta Vulcanol 3:21–68

Hübner JS, Sato M (1970) The oxygen fugacity-temperature relationships of manganese oxide and nickel oxide buffers. Am Mineral 55:934–952

Keller J (1982) Mediterranean island arcs. In: Thorpe RS (ed), Wiley , Chichester, pp 307–325

Keller J, Hornig-Kjarsgaard I, Koberski U, Stadlbauer E, Lenhard R (1993) Geological map of Stromboli 1:10000. Acta Vulcanol 3

Klug C, Cashman KV (1996) Permeability development in vesciculating magmas: implication for fragmentation. Bull Volcanol 58:87–100

Köhler TP, Brey GP (1990) Calcium exchange between olivine and clinopyroxene calibrated as a geothermobarometer for natural peridotites from 2 to 60 kb with applications. Geochim Cosmochim Acta 54(9):2375–2388

Kress VC, Carmichael ISE (1991) The compressibility of silicate liquids containing Fe_2O_3 and the effect of composition, temperature, oxygen fugacity and pressure on their redox states. Contr Mineral Petrol 108(1–2):82–92

Kretz R (1982) Transfer and exchange equilibria in a portion of the pyroxene quadrilateral as deduced from natural and experimental data. Geochim Cosmochim Acta 46:411–422

Kretz R (1983) Symbols for rock forming minerals. Am Mineral 68:277–279

Le Maitre RW, Bateman P, Dudek A, Keller J, Lameyre J, Le Bas MJ, Sabine PA, Schimd R, Sørensen H, Strekeisen A, Wolley AR, Zannettin B (1989) a classification of igneous rocks and glossary of terms. In: La Maitre RW (ed), Recommendations of the International Union of Geological Sciences Subcommission on the Systematics of Igneous Rocks, Blackwell Scientific Publications, Oxford, 193 pp

Loucks RR (1996) A precise olivine-augite Mg-Fe-exchange geothermometer. Contr Mineral Petrol 125(2-3):140–150

Mattioli M, Serri G, Salvioli-Mariani E, Renzulli A, Holm PM, Santi P, Venturelli G (2003) Subvolcanic infiltration and syneruptive quenching of liquids in cumuate wall-rocks: the example of the gabbroic nodules of Stromboli (Aeolian Islands, Italy). Mineral Petrol 78(3-4):201–230

Marquez A, Oyarzun R, Doblas M, Verma SP (1999) Alkalic (ocean-island basalt type) and calc-alkalic volcanism in the Mexican volcanic belt: A case for plume-related magmatism and propagating rifting at an active margin? Reply Geology 27(11):1056–1056

McBirney AR (1980) Mixing and unmixing of magmas. J Volcanol Geothermal Res 7: 357–371

Mercier JCC (1980) Single-pyroxene thermobarometry. Tectonophysics 70:1–37

Mercier JCC, Nicolas A (1975) Textures and fabrics of upper mantle peridotites as illustrated by xenoliths from basalts. J Petrol 16:454–487

Métrich N, Bertagnini A, Landi P, Rosi M (2001) Crystallization driven by decompression and water loss at Stromboli Volcano (Aeolian Islands, Italy). J Petrol 42:1471–1490

Morelli C, Giese P, Cassinis R, Colombi B, Guerra I, Luongo G, Scarascia S, Schutte KG (1975) Crustal structure of Southern Italy A seismic refraction profile between Puglia-Calabria-Sicily. Boll Geof Teor Appl 18:183–210

Nakamura N (1974) Determination of REE, Ba, Fe, Mg, Na and K in carbonaceous and ordinary chondrites. Geochim Cosmochim Acta 38:757–775

Nappi G (1976) L' Eruzione dello Stromboli del Novembre 1975. Boll Soc Geol It 95:991–1008

Newton RC, Charlo TV, Kleppa OJ (1980) Thermochemistry of the high structural state of plagioclase. Geochim Cosmoch Acta 75:369–376

Panza GF, Pontevivo A (2002) The lithosphere-astenosphere system in the Calabrian Arc and surrounding seas. The Abdus Salam international centre for theoretical physics (UNESCO- IAEA), pp 1–38

Papale P (1999) Modelling of the solubility of two-component H_2O-CO_2 fluid insilicate liquids. Am Mineral 84:477–492

Peccerillo A, Taylor SR (1976) Geochemistry of Eocene Calc-Alkaline volcanic rocks from Kastamorun area, Northern Turkey. Contrib Mineral Petrol 58:63–81

Peccerillo A (1999) Multiple mantle metasomatism in central-southern Italy: Geochemical effects, timing and geodynamic implications. Geology 27(4):315–318

Peccerillo A (2001) Geochemical similarities between the Vesuvius, Phlegraean Fields and Stromboli Volcanoes: petrogenetic, geodynamic and volcanological implications. Mineral Petrol 73(1–3):93–105

Reiners PW, Hammond PE, McKenna JM, Duncan RA (2000) Young basalts of the central Washington Cascades, flux melting of the mantle, and trace element signatures of primary arc magmas. Contrib Mineral Petrol 138(3):249–264

Renzulli A, Santi P (1997) Sub-volcanic crystallization at Stromboli (Aeolian Islands, southern Italy) preceding the Sciara del Fuoco sector collapse: evidence from monzonite lithic suite. Bull Volcanol 59:10–20

Renzulli A, Serri G, Santi P, Mattioli M, Holm PM (2001) Origin of high silica liquids at Stromboli volcano (Aeolian Islands, Italy) inferred from crustal xenoliths. Bull Volcanol 62:400–419

Renzulli A, Tribaudino M, Salvioli-Mariani E, Holm PM (2003) Cordierite-anorthoclase hornfels xenoliths in Stromboli lavas (Aeolian Islands, Sicily): an example of a fast cooled contact aureole. Eur J Mineral 15/ 4:665–679

Richet P, Bottinga Y, Denielou L, Petitet JP, Tequi C (1982) Thermodynamic properties of quartz, crystobalite and amorphous SiO_2: drop calorimetry measurements between 1000 and 1800°K and a review from 0 to 2000°K. Geochim Cosmochim Acta 46:2639–2658

Ripepe M, Gordeev E (1999) Gas bubble dynamics model for Shallow volcanic tremor at Stromboli. J Geoph Res 104(B5):10635–10654

Roeder PL, Campbell IH, Jamieson HE (1979) A Re-evaluation of the olivine-spinel geothermometer. Contrib Mineral Petrol 68:325–334

Rosi M, Bertagnini A, Landi P (2000) Onset of the persistent activity at Stromboli Volcano (Italy). Bull Volcanol 62:294–300

Sack RO, Ghiorso MS (1989) Importance of considerations of mixing properties in establishing an internally consistent thermodynamic database: thermochemistry of minerals in the system Mg_2SiO_4-Fe_2SiO_4-SiO_2. Contrib Mineral Petrol 102:41–68

Sisson TW, Grove TL (1993) Temperatures and H_2O contents of low-MgO high-alumina basalts. Contrib Mineral Petrol 113(2):167–184

Vaggelli G, Francalanci L, Ruggieri G, Testi S (2003) Persistent polybaric rests of calc-alkaline magma at Stromboli volcano, Italy: pressure data from fluid inclusions in restitic quartzite nodules. Bull Volcanol 65:385–404

Wood DA, Joron JL, Treuil M, Norry M, Tarney J (1979) Elemental and Sr isotope variations in basic lavas from Iceland and the surrounding ocean floor. Contrib Mineral Petrol 70:319–339

Wood BJ, Blundy JD (1997) A predictive model for rare earth element partitioning between clinopyroxene and anhydrous silicate melt. Contrib Mineral Petrol 129:166–181

Wood BJ, Blundy JD (2002) The effect of H_2O on crystal-melt partitioning of trace elements. Geochim Cmochim Acta 20:3647–3656